Proceedings of the 21st ICSMGE, Vienna, Austria, 14 – 19 June 2026. Pistrol, Adam & Schweiger (eds.)
Published by: ÖGG, Austrian Society for Geomechanics, Salzburg, Austria, ISBN 978-3-9503898-4-5
https://doi.org/10.53243/ICSMGE2026-1950

Impact of ITZ around unmixed soil-aggregates on hydraulic properties of earth levees material reinforced by deep soil mixing method

Myriam Duc, Alain Le Kouby, Sahar Hemmati
GERS-SRO, Université Gustave Eiffel, Champs-sur-Marne, France, myriam.duc@univ-eiffel.fr

Juba Amrioui
Laboratoire de Mécanique Gabriel Lamé, Polytech Tours, Tours, France

ABSTRACT: Deep soil mixing (DSM) method consisting in in-situ soil mixed with usually blast furnace slag-rich cement allows the strengthening and waterproofing of earth structures such as levees. However during implementation, the in-situ mixing until 10 meters depth may be uncomplete producing unmixed soil-aggregates in soil-cement matrix. Using collected intact cores bored on 4 sites in Loire river levees in France, the impact of the percentage of unmixed soil-aggregates coupled to the percentage of gravels (stones) higher than 2 mm in DSM material was demonstrated using hydraulic (K in m/s) measured using triaxial cell. Indeed, the K values increased clearly from 10^{-12} to 10^{-9} m/s with increasing unmixed soil-aggregates from 5 and 20%. This paper proposes a contribution to better characterize the role of inclusions (gravels or soft/dispersive unmixed soil-aggregates) and the potential role of Interface Transition Zone (ITZ) as usually observed around gravels in usual concrete. The DSM microstructure (especially ITZ) was observed using X-ray tomography, SEM, optical microscope on thin lamella, mercury intrusion porosimetry and phenolphthalein test coupled to color change under air exposure. The presence of ITZ was confirmed and characterized by a double layer structure and a complex shape considering dispersive properties of soil inclusions in cement matrix and by a large width reaching around 1 to 2 mm. Finally, the numerical calculations of hydraulic properties including such ITZ width matched with experimental water permeability measurement on site specimens.

KEYWORDS: interface transition zone, deep soil mixing, permeability, microscopic observations, unmixed soil aggregates, inclusion.

1 INTRODUCTION

Deep soil mixing (DSM) refers to a self-compacting mixture between in situ soil, cement and water. Used for levees waterproofing, the efficiency of the treatment is based on cement hydraulic properties. Contrary to concrete containing only stony aggregates (sand and gravels), the DSM implementation may induce the appearance of unmixed soil aggregates. Such 'soft' inclusions in well-mixed soil-cement matrix impact the mechanical and hydraulic properties of hardened DSM materials. In literature, authors studied the impact of inclusion using numerical or experimental approaches. To better estimate the hydraulic or mechanical properties especially in numerical approach, the Interfacial Transition Zone or ITZ located between the aggregates and the matrix (Winslow et al. 1994) was introduced as in usual concrete domain. ITZ is considered as a zone of mechanical weakness and higher water permeability in concrete due to its higher porosity compared to the surrounding cementitious matrix. So its presence in the concrete material can have consequences for the hydromechanical performance and durability of the concrete (Zimbelmann 1985; Liao et al. 2004). In the literature, the formation of ITZ in concrete is attributed to various mechanisms that occur during the setting and hardening of the material. These mechanisms include the wall effect of anhydrous cement grains against the relatively flat aggregate surface (Scrivener and Gartner 1987; Wang et al. 2021) as illustrated on Figure 1, the type and organization of hydrated products at interface compared to the hydrates formed in the matrix (Ollivier et al. 1995; Muslim 2020), the exchange of water and ions between the fresh matrix and the relatively porous aggregates (Ollivier et al. 1995; Kong and Du 2015), the 'one-sided growth' effect (Garboczi and Bentz 1991), the filtration effect or 'two-wall' effect (Lagerblad and Kjellsen 1999) as well as the 'micro-bleeding' effect (Zimbelmann 1987; Xu et al. 2022).

In standard Portland cement-based concrete, ITZ generally has a higher water ratio with fewer cement grains, resulting in a large amount of larger portlandite platelets and a deficit of CSH gel during the cement setting process. These characteristics explain the high porosity and permeability as well as the lower mechanical performance of ITZ compared to the surrounding cement matrix. The behavior of concrete at macroscopic scale, although influenced by the cementitious matrix performance and the aggregates characteristics, such as their nature, quantity, size, shape and spatial distribution, can also be affected by ITZ. Location for the development of initial cracks during mechanical loading (De Larrard and Belloc, 1999), ITZ also plays a crucial role in transport phenomena through hardened concrete.

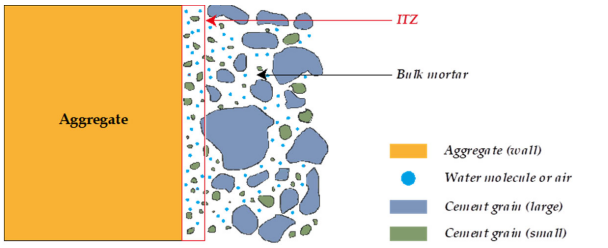

Figure 1. Illustration of the wall effect at ITZ zone (red square) before the setting and hardening process of concrete according to Scrivener et al. (2004) and Wang et al. (2021).

Since the relative volume of the ITZ is proportional to the external surface area of the aggregates, which depends on their volume fraction and particle size distribution (Bentz 2000), the greater the quantity of aggregates, the thinner the matrix. Above a critical volume fraction of aggregates, the ITZs, whose thickness depends on several factors such as the ratio in the matrix and the type of binder used, can overlap and form percolation paths that are less resistant to flow due to the high porosity and permeability in the ITZ (Winslow et al. 1994; Larbi et al. 2016). Results from numerical and experimental studies have shown that the critical volume fraction of aggregates is generally around 50%, with ITZs approximately 15 to 20 µm thick (Winslow et al. 1994; Garboczi and Bentz 1996; Shane et al. 2000; Zheng and Zhou 2007).

Watson and Oyeka (1981) observed that the permeability of concrete containing between 55 and 75% aggregates was approximately 100 times higher than that of the matrix, with E/C ratios ranging from 0.3 to 0.8. Moreover, Nyame (1985) found an increase in the permeability of a mortar with a E/C ratio of 0.47 when the sand fraction varied between 20 and 70%, despite a decrease in the total porosity accessible to water.

If studies have focused on usual concrete behavior, no paper has confirmed the presence of an interfacial transition zone (ITZ) around soil-based aggregates in deep soil mixing materials. The present study aims to characterize ITZ in DSM materials, combining experimental observation and a numerical approach demonstrating ITZ impact on hydraulic properties that govern the material durability.

2 MATERIALS AND METHODS

2.1 *Materials*

Vertical core samples with a 100 mm diameter were taken at depths of 6-8 m in DSM cut-off walls realized in 5 dyke construction sites along the Middle Loire in France. The test specimens were stored at 20°C with 100%RH in a double airtight envelope to prevent drying. Despite these precautions, browning of the initially bluish cement matrix was observed on the surface of the samples when exposed to air during storage indicating a possible surface drying.

Table 1 shows the different sites where core samples named SC1-M, SC2-S, SC3-R, SC4-G and SC4-S. Information on the year of construction of the DSM cut-off walls, the applied soil mixing technique (humid method: cementitious grout mixed with soil, dry method: anhydrous cement in situ mixed with soil and water with CEM III/C rich with 85% blast furnace slag), the geotechnical properties of site soil, and the formulation parameters such as cement C and water dosage E are also provided. Only the water added during mixing was measured, while the natural water content of the mixed soils was estimated around 20 to 25%.

Table 1. Tested materials origins and characteristics

	SC1-M	**SC4-G**	**SC4-S**	**SC2-S**	**SC3-R**
Frabric year	2017	2013	2013	2018	2021
DSM method	Dry	Dry	Humid	Dry	Dry
Year of lab test	2021	2021	2021	2021	2021
$\boldsymbol{C}$ (kg/m^3)	206	218	329	222	230
E_{add} (kg/m^3)	314	424	468	297	390
CaO add (kg/m^3)	-	-	-	19	-
$\boldsymbol{E/(C+CaO)}$	1.52	1.95	1.42	1.23	1.70
W_{added} (%)	18	31	40	17	27
Estim. W_{tot} (%)	38-43	51-56	60-65	37-42	47-52
0/80 µm (%)	25	48	62	58	68
0/2 µm (%)	8	18	26	21	16
LL (%)	22	25	32	30	n.m
MB (g/100g)	0.7	0.8	1.9	2.4	1.4-3

2.2 *Methods*

The porosity and pore size distribution of the DSM material previously soaked in liquid nitrogen and freeze-dried (at T°C = -52 °C and P = 0.07 mbar) was measured using an AutoPore IV Micrometrics mercury intrusion porosimeter or MIP (P = 0.0035 to 412.8 MPa, 10 s and 30 s = time equilibrium times at low and high pressure, σ_{Hg}=0.485 N.m^{-1} and θ_{Hg}=141°). The alkalinity level of the material was evaluated by performing a phenolphthalein test on the fresh fractured surfaces of DSM materials.

Observations were made using a digital depth-of-field microscope (Keyence VHX-7000) on thin slices (under natural light as in petrography) prepared from DSM material collected from the site around unmixed soil-aggregates, then embedded in resin and thinned to a thickness of 30 µm. Other larger samples were embedded in resin, cut and polished to obtain a smooth and flat surface for observing the cemented matrix microstructure and ITZ area using a QUANTA 400 FEI environmental scanning electron microscope (E-SEM) coupled with an EDX probe.

X-ray Computed Tomograph (Ultratom from RX Solutions) was used to visualize the 3D microstructure of sample without destructive preparation (source L10801 Hamatsu, PaxScan4343DX-I imager, source: 200 kV/300 µA). As X-ray absorption coefficient depends strongly on the density and chemical composition of the material, with a photoelectric absorption probability proportional to $(Z/E)^3$ (with Z the atomic number of the phase traversed by X-ray at a given energy E), it is possible to discriminate the different phases composing DSM materials, i.e. the well-mixed soil-cement matrix, gravel, as well as macroporosity and cracks. Only components larger than 30 µm were distinguished while soil inclusions were not clearly observed due to their close density to well-mixed soil-cement matrix.

For hydraulic measures, cylindrical test specimens (D = 50 mm and H = 100 mm) were cut under water using a saw. The water permeability tests were carried out using a triaxial cell following the XP CEN ISO/TS 17892-11 standard (AFNOR, 2005) and water-accessible porosity tests followed the NF P94-410-3 standard (AFNOR, 2001).

Finally a geometric model was generated based on the concept of the random aggregate structure (RAS) assimilating aggregates to spheres with a random aggregates position (without overlapping and no contact), while respecting the experimental soil aggregate/gravels size distribution in specimen. The RAS concept was applied considering that unmixed soil aggregates were not distinguished on X-ray tomographic specimen 3D-reconstruction. The artificial geometric model (Figure 2) was introduced into the Model Builder interface of COMSOL Multiphysics and the finite element (FE) model was created with four components whose characteristics are described in Table 2 and detailed in Amrioui (2023). ITZ with a 1000 µm thickness around unmixed soil inclusions and a 500 µm one around gravels was chosen (parameters validated by experimental observation in the present paper).

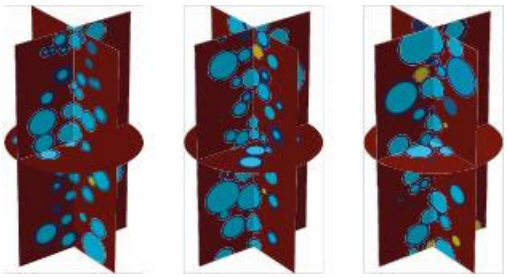

Figure 2. Some examples of the four-phase geometric models 3D-RAS-ITZ generated to estimate the water permeability of in situ DSM materials: (Red) Soil-cement matrix; (Light blue) Unmixed soil inclusions; (Yellow) Gravel; (Dark blue) ITZ

Table 2. Tested materials characteristics (Amrioui 2023)

Materials	soil-cement matrix		Unmixed soil aggregates		Gravels	
	Km (m/s)	Pm (%)	Ks (m/s)	Ps (%)	Kg (m/s)	Pg (%)
SC1-M	1,2E-11	35,0	5,5E-07	31,7	3,0E-13	8,5
SC2-S	1,3E-11	40,2	1,2E-07	30,1	3,0E-13	8,5
SC3-R	9,1E-11	59,9	2,4E-07	34,5	3,0E-13	8,5
SC4-G	5,4E-11	49,3	2,0E-07	32,3	3,0E-13	8,5
SC4-S	1,6E-11	46,8	3,1E-07	30,1	3,0E-13	8,5

As the local porosity of ITZ as well as water permeability remained undetermined from experiment given the resolution limit of apparatus, a parametric study was carried out to assess the influence of this parameter on the effective permeability of DSM materials and adjust it to bring it closer to the experimental results, while comparing it to values found in the literature for concrete. Shane et al. (2000) reported that the water permeability of the ITZ should be higher than that of the bulk matrix, with a ratio of up to 10 to 100 times higher.

The water permeability test was simulated using previous model called 3D-FS-ITZ by applying boundary conditions to create a constant upward water flow through the geometric structure in the Model Builder interface. A negative pressure of 100 kPa was created by applying two different pressures: a pressure of 200 kPa at the bottom of the test specimen and atmospheric pressure of 100 kPa at the top. The side surface of the test specimen, which was in contact with the membrane used in triaxial cell in lab test, was considered waterproofed.

3 RESULTS

3.1 *Water porosity and permeability of DSM materials*

Porosity may come from the soil cement matrix (spaces between particles increasing with low cement content), porous unmixed soil aggregates, ITZ and interfaces, microcracks during hardening (drying) or air trapped bubbles during implementation. The last two porosities (macropores) was observed and estimated by X-ray tomography (Figure 3).

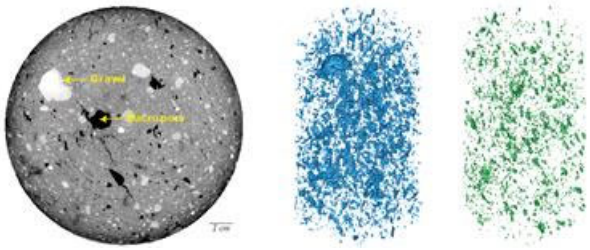

Figure 3. 2D X-ray tomographic image and 3D macroporosity organization (between 1 and 15 mm) in DSM samples from sites after reconstruction from the 2D stacked images. Left to right: SC1-M-P 2.98m depth (P_{macro} = 4,1%), SC4-S-P 5.03m depth (P_{macro} = 0,6%)

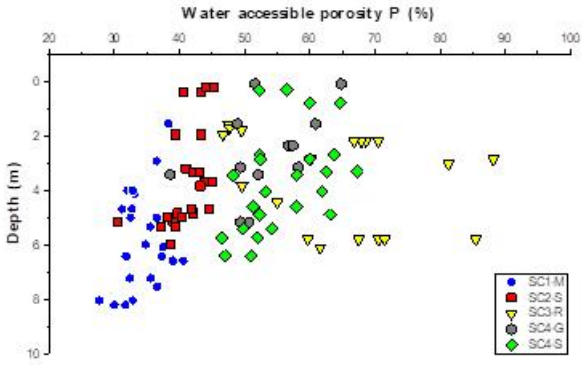

Figure 4. Water porosity in DSM materials versus the depth of collect in in-situ cut-off wall in levee.

Parallel to the macroporosity, micropores and nanopores varied during the DSM implementation considering the soil clay content whose quantity was estimated through the methylene blue value (MB) in Table 1. Higher clay content made the mixing more or less uncomplete between soil and cement conducting to increasing unmixed soil inclusions fractions noted P_{3D}^{S} (Amrioui et al. 2023b). Correlated to the clay content in soil, the water accessible porosity in DSM material in Figure 4 appeared maximum in SC3-R (P > 50%) accompanied by almost no gravels and minimum in SC1-M (P= 25-40%) with more than 5% gravels. Figure 5a show two water permeability trends in DSM materials for more or less clay rich soil (K= 3.10^{-12} to 10^{-9} m/s) characterized by either a bimodal porosity or a monomodal porosity, respectively. If low gravels fraction less than 5% didn't seem impacting the permeability trend on Figure 5b, an increasing gravel fraction beyong such content seemed correlated to lowering permeabilities.

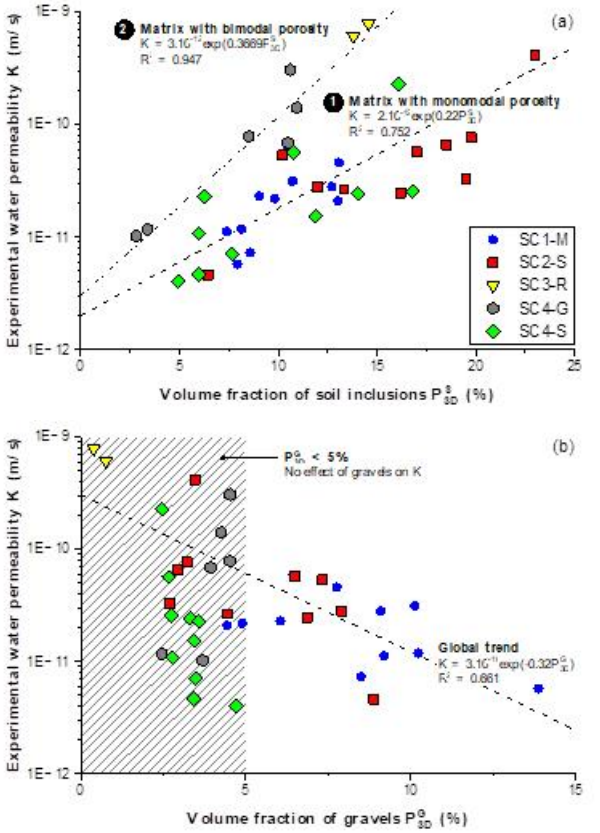

Figure 5. Variation in water permeability K versus: (a) volume fraction of unmixed soil inclusions noted P_{3Ds}; (b) Volume fraction of gravel noted P_{3Dg}

3.2 *Macroscopic observation of the brunishing of the specimen surface*

The porosity of cement paste and the presence of ITZ around unmixed soil aggregates in DSM material were not only observed at microscale but also at macroscale. Indeed, a color change (from blue to the natural brown soil color) usually affected area with an average thickness of approximately 1 to 2 mm around inclusions, as shown on Figure 6. This discoloration phenomenon was also observed by Helson (2017) on DSM mixtures containing Speswhite kaolinite, Fontainebleau sand and CEM III/C, subjected to humidification/drying cycles. The discolored area should correspond to carbonated zone, whose the boundary was highlighted by a phenolphthalein test. Indeed, when the DSM material was partially dried, carbon dioxide from air enters the material via pore desaturation, causing calcium carbonate ($CaCO_3$) precipitation. The usual white colored particles of carbonate should contribute to the color change. As Helson, phenolphthalein test applied on the tested DSM in the present study showed a decrease in pink intensity caused by CO_2 flow through unsaturated pores in material after 1 month storage contributing the slow surface discoloration (Figure 7). The carbonation hypothesis was reinforced by the slight decrease of macropores sizes (filled by carbonates) observed on a soil

cement matrix before and after air contact (Figure 8). At the opposite, Hessouh (2021) observed that the brown area appearing on a soil mixed with CEM III/C and lime remained pink-stained after a phenolphthalein test suggesting a non-carbonated area. Such results confirms, as suggested by Le Cornec et al. (2017), that the discoloration was also linked to the simultaneous oxygen penetration in desaturated pore (accompanied by CO_2). Oxygen (as an oxidant) may react with sulfide ions S^{2-} and S^{3-} (reduced forms of sulfur contained in CEMIII cement) to form sulfate, inducing the color change of cemented matrix as confirmed by Zhang et al. (2025). The discoloration not only concerned the exposed surface to air but also the interface between soil-cement matrix and inclusion suggesting a higher porosity in such area, as well as a high connectivity between pores until ambient air.

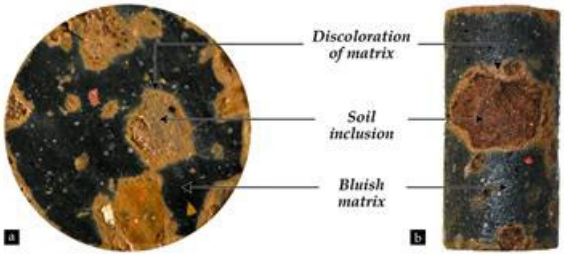

Figure 6. Illustration of the disappearance of the bluish coloration around the soil inclusions in DSM matrix.

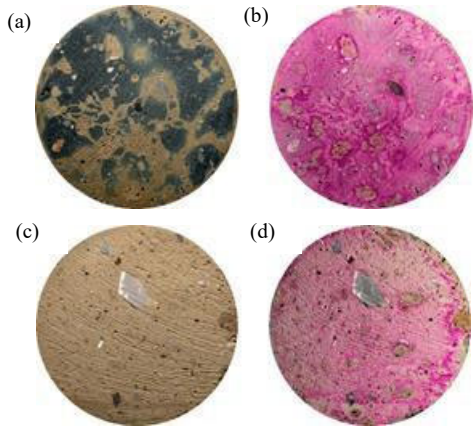

Figure 7. Phenolphthalein test on SC3-R sample performed immediately after extraction from soil (a-b) and after 1 month of storage under endogenous conditions (c-d).

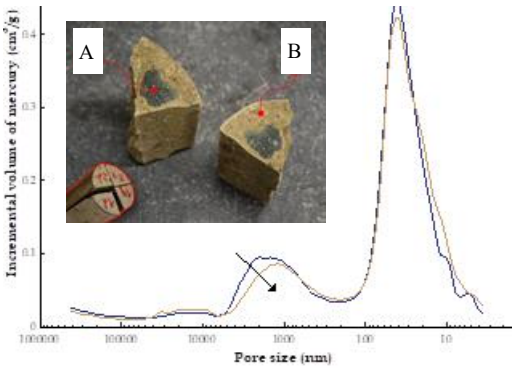

Figure 8. Pore size distribution in DSM material measured by MIP test on A (blue line): bluish area (P= 50.1%), B (brown area): discolored area (P=48.8%). The soil mixed with cement contains a clay-rich soil at the origin of the high total porosity.

3.3 *Observation of ITZ under SEM and optical microscope*

Figure 9 highlights a matrix-inclusion interface and a matrix-gravel interface using SEM. The quartz grain/cemented matrix interface at high magnification on Figure 9a shows a crack opening of a few micrometers, coming probably from the matrix shrinkage during the clay-rich sample drying or the preparation before observation.

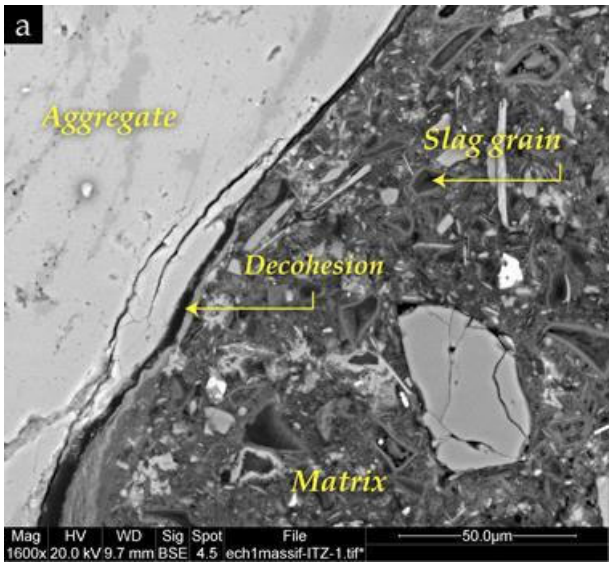

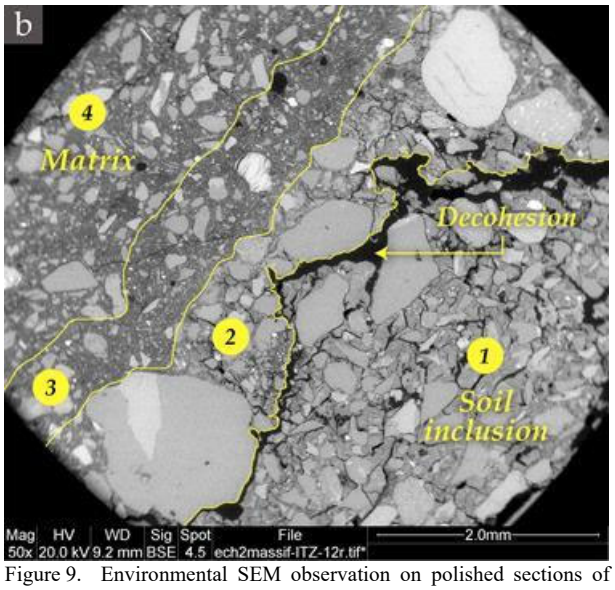

Figure 9. Environmental SEM observation on polished sections of DSM embedded in resin: (a) matrix-inclusion interface; (b) matrix-granule interface

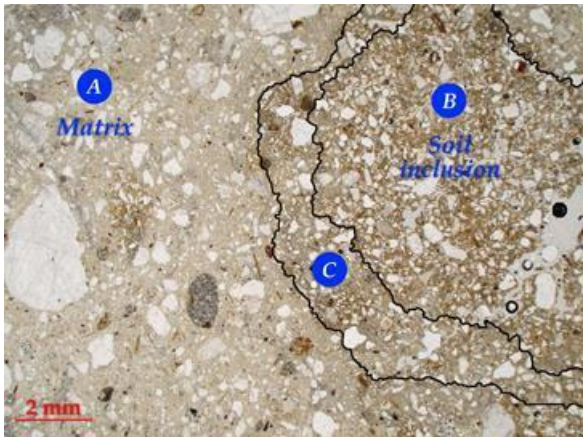

Figure 10. Observation with optical microscope of a thin section of a DSM material from site embedded in resin, highlighting the well-mixed soil-cement matrix/ unmixed soil inclusion interface.

Visible black particles with angular shape corresponding to a depression and surrounded by a thin light grey layer were likely to be slag grains with an average size of around 10 µm surrounded by precipitated cementitious hydrates mixed with clay particles that may disperse more or less in the cement grout.

Around unmixed soil aggregate on Figure 9b SEM revealed 4 zones while the thin section observed by optical microscopy (Figure 10) allowed distinguishing only 3 zones based on the brown-color level:

Area (1) (associated to B area): corresponds to the unmixed soil aggregates characterized by mainly close particles (in light grey) separated by microcracks (uncemented soil),

Area (4) (associated to A area): rather associated to greyish color, such area mainly represents the well-mixed soil-cement matrix with well dispersed light grey particles (sand) in dark grey cement matrix.

Area (2) (associated to C area): at interface in contact with unmixed soil aggregates, area with an average thickness of a few hundred micrometers, appeared to be less cracked than the soil inclusion but less compact than the soil-cement matrix. The penetration of cement into the superficial layer of soil aggregates made such area more resistant than the inner zone of soil inclusion. As a proof, huge crack (in black) appeared at area (2) boundary,

Area (3) (unclear area under optical microscope): area is characterized by a lower concentration of sand grains compared to the cemented matrix (4), with an average thickness of approximately 1000 µm. This phenomenon can be explained by the rotational movement of the undisintegrated soil inclusions within the DSM matrix in fresh fluid state during the mixing process. A shear zone must therefore be created between the unmixed soil bullets and the binder phase, associated to the well-mixed soil-cement matrix.

Finally, observations allowed to discern a well-defined interface associated to ITZ zone between the soil inclusion and the rest of the matrix. Based on the clear difference in porosity between the well-mixed matrix (4 - A) and inclusion (1 - B), the ITZ zone corresponds to the double layer (2)-(3) (corresponding to the C area) with a 1-2 mm average width.

3.4 *Numerical simulation of hydraulic properties*

The numerical simulation of hydraulic properties allowed to calculate the permeability K of DSM specimen containing gravels and unmixed soil aggregates and to compare it to the experimental value (Figure 11).

First calculations (Figure 11a) only considered the soil/cement matrix (m) properties (without inclusions or gravels) as the smallest porosity interconnecting pores with higher sizes, mainly control the water permeability in whole material. The model developed by Katz and Thompson (1987) was applied to estimate K_m (Amrioui et al. 2023a). Estimated K_m values fitted well the experimental ones in several materials but not for all, as some points didn't reach the grey domain on Figure 11, defined by A value lower than 5 (A corresponds to a criteria to appreciate the goodness of fit).

Considering now gravels and unmixed soil aggregates spread in the matrix according to the Figure 2, with ITZ widths fixed at 1000 and 500 µm around unmixed soil inclusions and gravels respectively, the numerical modeling of DSM water permeability K_{num} was highly improved. Indeed the whole estimations (17 points) became closer to the experimental measures on Figure 11b. For calculations, an estimation of the specific water permeability in ITZ was required. As such measure remained inaccessible by technical ways, a b-factor was introduced (b corresponds to efficiency factor of the simulated parameter (here K) as introduced by Li et al. (2016a, 2016b) or Liang et al. (2020). The b factor was defined as the ratio between K_{ITZ} and K_m. and was fixed at 20 for 3D simulations (after a parametric study), while 2D simulations on Figure 12 were realized with a b factor equal to 100. Such overestimated value allowed to highlight the ITZ width effect on the development of preferential water flow channels in DSM material, when ITZ overlapped. Such overlapping effect may represent a harmful phenomenon for waterproof DSM cut-off wall implemented in levee bodies.

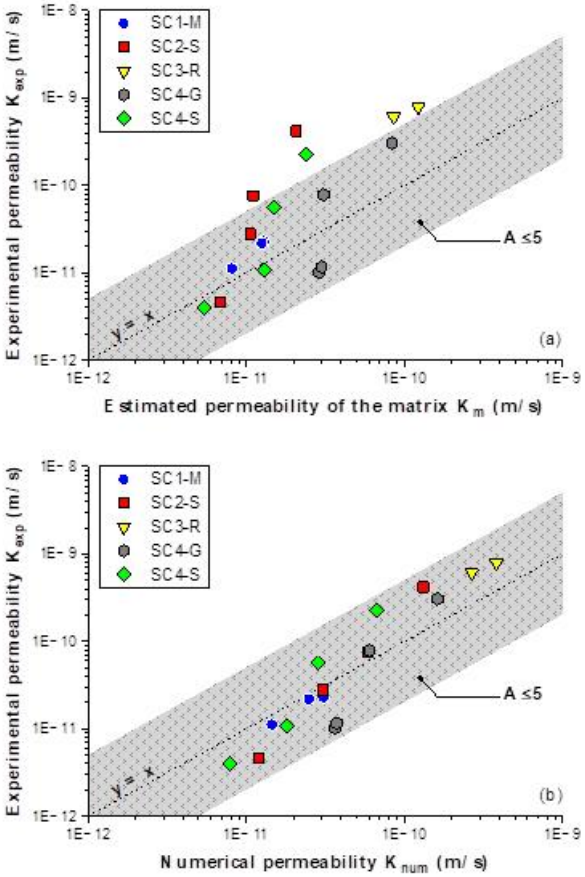

Figure 11. Experimental water permeability measured experimentally on DSM test specimens versus: (a) Water permeability of the matrix alone estimated using the model developed by Katz and Thompson (1987); (b) Water permeability calculated using the 3D-RAS-ITZ geometric model introduced in COMSOL Physics software.

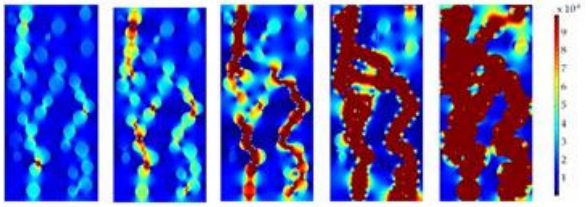

Figure 12. Example of 2D numerical modeling using RAS concept (inclusion assimilated to sphere with uniform size): water flow velocity fields in DSM material with an unmixed soil-cement fraction equal to 25%, and a *b*-factor equal to 100 and the introduction of ITZ with different thicknesses from left to right: 100 µm; 500 µm; 1000 µm (observed width); 2000 µm; 3000 µm

4 CONCLUSIONS

The observations at micro/microscale of DSM materials from site (composed by more or less clay-rich soil, CEMIII/C and water) confirmed the presence of ITZ around unmixed soil aggregates, as observed and described in usual concrete

containing gravels. Contrary to ITZ around gravel, such area appeared as a double layer composed by a cemented soil (induced by the cement superficial penetration into the soil aggregates) and a cemented matrix layer characterized by sand grain depletion.

The average width of ITZ was evaluated around 1 to 2 mm, which allowed to reach a good matching between numerical calculation and experimental measurement of water permeability K of DSM materials. For numerical approach, a specific geometry was introduced in COMSOL Multiphysics software based on RAS concept and experimental size distribution of inclusions, referring to gravels and unmixed soil aggregates. The last ones assimilated to spheres, were rounded by a 1 mm width ITZ as uniform layer corresponding to the observed width.

The water permeability in various DSM materials reached 10^{-9} to 5.10^{-11} m/s considering the macroporosity observed by X-ray tomography but also the microporosity in cement matrix and in ITZ. Such porosity connects the specimen interior to the outside ambient air, inducing the specimen carbonation (under CO_2 gas penetration) accompanied by a discoloration of the initial bluish blast furnace slag-rich CEMIII/C matrix (associated to sulfur oxidation). Such porosity reaching usually 30 to 70% may be at the origin of gas flow in material (during desaturation) but also lixiviation (with calcium loss under saturation state) conducting to possible pathology or degradation in cut-off wall. The loss of efficiency in term of permeability may then result in premature maintenance to prevent failure of river levee.

5 ACKNOWLEDGEMENTS

The Navier laboratory (France) was thanks for X-ray tomographic observations while the petrographic thin section was prepared by thin Section lab (Toul, France).

6 REFERENCES

AFNOR, 2005. Reconnaissance et essais géotechniques - Essais de laboratoire sur les sols - Partie 11 : détermination de perméabilité à charge constante et à charge variable décroissante. French National standards XP CEN ISO/TS 17892-11.

AFNOR, 2001. Roches - Essais pour déterminer les propriétés physiques des roches - Partie 3 : détermination de la porosité. French National standards. NF P94-410-3.

Amrioui, J., Le Kouby, A., Duc, M., Guedon, J. -S., Lansac, F. 2023a. Relationship between Porosity and Water Permeability for Deep Soil Mixing Material. *International Journal of Geomechanics* 23(7), 04023086.

Amrioui, J., Duc, M., Le Kouby, A., Guedon, J. -S., Saussaye L., Hemmati S., Willot S., Dokladal P. Lansac, F. 2023b. Characterization by image analysis of materials heterogeneities produced by the Deep Soil Mixing technique. *Materials Today: Proceedings*. Available at: https://hal.archives-ouvertes.fr/hal-04385930

Amrioui, J. 2023, Vulnérabilité des digues au changement climatique : approche multi-échelle pour l'étude du comportement à long terme des mélanges sol-ciment et effet des inclusions de sol non traité lors du processus de malaxage. PhD thesis of University Gustave Eiffel, France.

Bentz, D. P. 2000. Fibers, percolation, and spalling of high-performance concrete. *Materials Journal* 97(3), 351-359.

De Larrard, F., Belloc, A. 1999. L'influence du granulat sur la résistance à la compression des bétons. *Bulletin des laboratoires des ponts et chaussées* 219.

Garboczi, E. J., Bentz, D. P. 1991. Digital simulation of the aggregate–cement paste interfacial zone in concrete. *Journal of materials Research* 6(1), 196-201.

Hessouh, J. J. 2021. Caractérisations physique et mécanique, et durabilité des bétons de sol: matériaux de laboratoire et matériaux de chantiers. PhD thesis of Cergy Pontoise, France.

Helson, O. 2017. Comportement thermo-hydro-mécanique et durabilité des bétons de sol: influence des paramètres de formulation et conditions d'exposition. PhD thesis of University Cergy Pontoise, France.

Katz, A. J., Thompson, A. H. 1987. Prediction of rock electrical conductivity from mercury injection measurements. *Journal of Geophysical Research: Solid Earth* 92(B1), 599-607.

Kong, L., Du, Y. 2015. Interfacial interaction of aggregate-cement paste in concrete. *Journal of Wuhan University of Technology-Mater. Sci. Ed*. 30(1), 117-121.

Larbi, B., Dridi, W., Dangla, P., Le Bescop, P. 2016. Link between microstructure and tritiated water diffusivity in mortars: Impact of aggregates. *Cement and Concrete Research* 82, 92-99.

Le Cornec D., Wang Q., Galoisy L., Renaudin G, Izoret L., Calas G. 2017, Greening effect in slag cement materials, *Cement and Concrete Composites* 84, 93-98.

Li, X., Xu, Y., & Chen, S. 2016, Computational homogenization of effective permeability in three-phase mesoscale concrete. *Construction and Building Materials* 121, 100-111.

Li, X., Xu, Q., & Chen, S. 2016b, An experimental and numerical study on water permeability of concrete. *Construction and building materials* 105, 503-510.

Liang, M., Feng, K., He, C., Li, Y., An, L., & Guo, W. 2020, A meso-scale model toward concrete water permeability regarding aggregate permeability. *Construction and Building Materials* 261, 120547.

Liao, K. Y., Chang, P. K., Peng, Y. N., & Yang, C. C. (2004). A study on characteristics of interfacial transition zone in concrete. *Cement and Concrete research* 34(6), 977-989.

Muslim, F. A. 2020. Review on The Microstructure of Interfaces in Reinforced Concrete and Its Effect on The Bond Strength. *CSID Journal of Infrastructure Development*, 3(1), 102-113.

Nyame, B. K. 1985. Permeability of normal and lightweight mortars. *Magazine of Concrete Research* 37(130), 44-48

Ollivier, J. P., Maso, J. C., Bourdette, B. 1995. Interfacial transition zone in concrete. Advanced cement-based materials, 2(1), 30-38.

Scrivener, K. L., & Gartner, E. M. 1987. Microstructural gradients in cement paste around aggregate particles. *MRS Online Proceedings Library (OPL)* 114, 77.

Scrivener, K. L. 2004. Backscattered electron imaging of cementitious microstructures: understanding and quantification. *Cement and concrete Composites* 26(8), 935-945.

Shane, J. D., Mason, T. O., Jennings, H. M., Garboczi, E. J., Bentz, D. P. 2000. Effect of the interfacial transition zone on the conductivity of Portland cement mortars. *Journal of the American Ceramic Society* 83(5), 1137-1144.

Wang, B., Yan, L., Fu, Q., Kasal, B. 2021. A comprehensive review on recycled aggregate and recycled aggregate concrete. *Resources, Conservation and Recycling* 171, 105565.

Watson, A. J., Oyeka, C. C. 1981. Oil permeability of hardened cement pastes and concrete. *Magazine of Concrete Research* 33(115), 85-95

Winslow, D. N., Cohen, M. D., Bentz, D. P., Snyder, K. A., Garboczi, E. J. 1994. Percolation and pore structure in mortars and concrete. *Cement and concrete research* 24(1), 25-37.

Zhang, Y., He, S., Liang, X., Liang, M., Çopuroğlu, O., Schlangen, E., 2025. Characterization of the transitional zone between fully carbonated and non-carbonated areas in slag-rich cement paste after long-term natural exposure. *Cement and Concrete Research* 198. Available at: https://doi.org/10.1016/j.cemconres.2025.107986.

Zheng, J., Zhou, X. 2007. Percolation of ITZs in concrete and effects of attributing factors. *Journal of materials in civil engineering* 19(9), 784-790.

Zimbelmann, R. 1985. A contribution to the problem of cement-aggregate bond. *Cement and concrete research* 15(5), 801-808.